Biotechnology Reports 3 (2014) 73–85

Contents lists available at ScienceDirect

Biotechnology Reports

journal homepage: www.elsevier.com/locate/btre

Crystal structure of *Clostridium acetobutylicum* aspartate kinase (*Ca*Ak): An important allosteric enzyme for amino acids production

Babu A. Manjasetty [a,b,*], Mark R. Chance [c,d], Stephen K. Burley [e], Santosh Panjikar [f], Steven C. Almo [g,**]

[a] European Molecular Biology Laboratory, Grenoble Outstation, 71 Avenue des Martyrs, Grenoble Cedex 9, 38000, France
[b] Unit of Virus Host-Cell Interactions (UVHCI), UJF-EMBL-CNRS, UMI 3265, 71 Avenue des Martyrs, Grenoble Cedex 9, 38000, France
[c] Center for Synchrotron Biosciences, National Synchrotron Light Source, Brookhaven National Laboratory, Upton, NY 11973, USA
[d] Center for Proteomics and Bioinformatics, School of Medicine, Case Western Reserve University, Cleveland, OH 44106, USA
[e] Center for Integrative Proteomics Research, Rutgers University, Busch Campus, 174 Frelinghuysen Road, Piscataway, NJ 08854-8076, USA
[f] Australian Synchrotron, 800 Blackburn Road, Clayton, Victoria 3168, Australia
[g] Department of Biochemistry, Albert Einstein College of Medicine, Bronx, NY 10461, USA

ARTICLE INFO

Article history:
Received 6 March 2014
Received in revised form 10 June 2014
Accepted 23 June 2014
Available online 25 June 2014

Keywords:
Aspartate kinase
Feedback inhibition
X-ray diffraction
Biosynthesis of amino acids

ABSTRACT

Aspartate kinase (AK) is an enzyme which is tightly regulated through feedback control and responsible for the synthesis of 4-phospho-L-aspartate from L-aspartate. This intermediate step is at an important branch point where one path leads to the synthesis of lysine and the other to threonine, methionine and isoleucine. Concerted feedback inhibition of AK is mediated by threonine and lysine and varies between the species. The crystal structure of biotechnologically important *Clostridium acetobutylicum* aspartate kinase (*Ca*AK; E.C. 2.7.2.4; Mw = 48,030 Da; 437aa; SwissProt: Q97MC0) has been determined to 3 Å resolution. *Ca*AK acquires a protein fold similar to the other known structures of AKs despite the low sequence identity (<30%). It is composed of two domains: an N-terminal catalytic domain (kinase domain) and a C-terminal regulatory domain further comprised of two small domains belonging to the ACT domain family. Pairwise comparison of 12 molecules in the asymmetric unit helped to identify the bending regions which are in the vicinity of ATP binding site involved in domain movements between the catalytic and regulatory domains. All 12 *Ca*AK molecules adopt fully open T-state conformation leading to the formation of three tetramers unique among other similar AK structures. On the basis of comparative structural analysis, we discuss tetramer formation based on the large conformational changes in the catalytic domain associated with the lysine binding at the regulatory domains. The structure described herein is homologous to a target in wide-spread pathogenic (toxin producing) bacteria such as *Clostridium tetani* (64% sequence identity) suggesting the potential of the structure solved here to be applied for modeling drug interactions. *Ca*AK structure may serve as a guide to better understand and engineer lysine biosynthesis for the biotechnology industry.

1. Introduction

Among plant amino acid biosynthesis pathways, the aspartate-derived amino acid pathway has received much attention by researchers because of the nutritional importance [1]. This pathway is responsible for the synthesis of essential amino acids such as isoleucine, lysine, methionine, and threonine starting from aspartate and therefore is commonly called aspartate-derived amino acids (Scheme 1a) [2]. Since asp-derived pathway does not exist in bacteria, fungi, humans and other animals, they depend on plants as the source of these essential amino acids. The first enzyme of the pathway is aspartate kinase (AK; E.C. 2.7.2.4) is leading to the synthesis of multiple end products and their biosynthetic intermediates controlled by feedback inhibition. AK catalyzes the first step i.e., transfer of the γ-phosphate group of ATP to aspartate and responsible for the formation of aspartyl-4-phosphate (Scheme 1b).

The aspartate kinase enzymes exhibit complex allosteric regulation. For instance, in *Arabidopsis thaliana* which contains five AKs, three of them are mono-functional AKs subjected to

* Corresponding author at: European Molecular Biology Laboratory, Grenoble Outstation, 6 rue Jules Horowitz, 38042 France. Tel.: +33 4 3888 1997; fax: +33 4 7620 7199.
** Corresponding author at: Department of Biochemistry, Albert Einstein College of Medicine, 1300 Morris Park Avenue, Bronx, NY 10461, USA.
E-mail addresses: babu@embl.fr, babu.manjasetty@gmail.com (B.A. Manjasetty), steve.almo@einstein.yu.edu (S.C. Almo).

http://dx.doi.org/10.1016/j.btre.2014.06.009

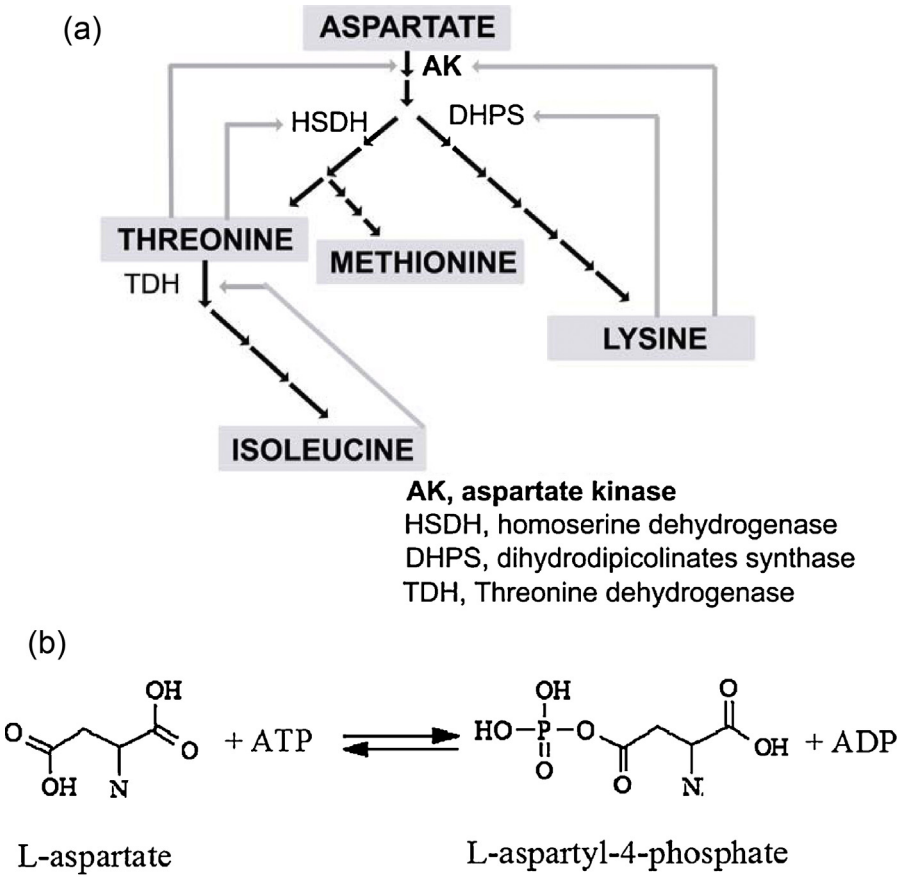

Scheme 1. a Schematic representation of the branched pathway in *Clostridium acetobutylicum* for synthesis of lysine, methionine, threonine and isoleucine from aspartate. Arrows represent multiple enzymatic steps. Feedback inhibition by threonine and lysine on aspartate kinase was showed in gray lines. Scheme 1b reaction catalyzed by aspartate kinase. Schematic diagram generated using the program ISIS/Draw [59].

feedback inhibition by lysine and S-adenosylmethionine (SAM) and the other two are bi-functional AKs conjugated with-homoserine dehydrogenase (HSDH) subjected to the feedback inhibition by threonine and leucine [3]. In *Escherichia coli* which contains three AK isozymes (two bi-functional and one monofunctional), however, only two of them are involved in allosteric control [4]. Three isoforms of AKs are also found in *Bacillus subtilis* [5,6]. Simpler allosteric regulation also exists in some organisms; *Methanococcus jannashii* and *Thermus thermophilus* contain only one AK which synthesizes only threonine [7] whereas in *Synechocystis* and *Corynebacterium glutamicum* the pathway leads to the synthesis of both threonine and lysine [8,9]. *Mycobacterium tuberculosis* exhibits a single isoform and potential feedback inhibiton mechanisms are not known [10]. The evolution of different types of AKs (monofunctional or bifunctional) and their phylogenetic relationships were described recently [11]. The allosteric regulation in this pathway, which involves not only downstream metabolites in the aspartate-derived amino acids, but also seemingly unrelated substances, provides precursors for the biosynthesis of other essential plant metabolites. This suggests that aspartate kinase is an important checkpoint for balancing the relative flux of different plant amino acid biosynthesis pathways [1,12]. Several metabolic intermediates of this pathway play major roles in quorum sensing [13,14], bacterial sporulation [15], methylation reaction [16] and cell wall crosslinking [17]. For example, an intermediate of lysine biosynthetic branch, meso-diaminopimelate is also a component of the peptidoglycan which is an essential component for cell wall synthesis. Interruption of the production of lysine and cell wall formation, by inhibiting aspartate kinase activity, is well established [18]. Depending upon the organism selected, metabolic branch point variation is observed [19].

Clostridium acetobutylicum is widely used organism in biotechnology industry, its genome has recently been sequenced and analyzed, and a database of the predicted protein complement has been published [20,21]. In view of its diversity and complexity in the allosteric control in variety of species, AK from *C. acetobutylicum* (*Ca*AK) was targeted for structure function analysis. *Ca*AK gene encodes a protein of 437amino acids with a predicted molecular mass of 48,030 Da (SwissProt:Q97MC0; PSI TargetTrack: NYSGXRC-6204b). An enzyme *Ca*AK is homologous to the pathogenic (toxin producing) bacteria *Clostridium tetani* aspartate kinase (*Ct*AK; spQ891L5; 64% identity) and *Clostridium perfringens* aspartate kinase (*Cp*AK; spQ8XJS6; 25% identity) suggesting the potential to be a possible drug target for these organisms (Fig. 1). Further, AKs are key enzymes controlling the biosynthesis of industrially important family of amino acids and deciphering the mechanism of end-product feedback inhibition of these allosteric enzymes is an essential issue for the development of highly efficient microbial strains for bio-production. Also, AKs has a very important biotechnological potential as it can limit the content of an essential amino acid (lysine) in cereals [22]. Sequence analysis of *Ca*AK suggests that it comprised of two domains, namely, N-terminal conserved amino acid kinase domain (Pfam PF00696) considered as catalytic domain indicates that *Ca*AK belongs to amino acid kinase family. This domain is further divided into two lobes, the N-lobe making up the Asp-binding site and the C-lobe providing a nucleotide-binding pocket for ATP. A second domain of

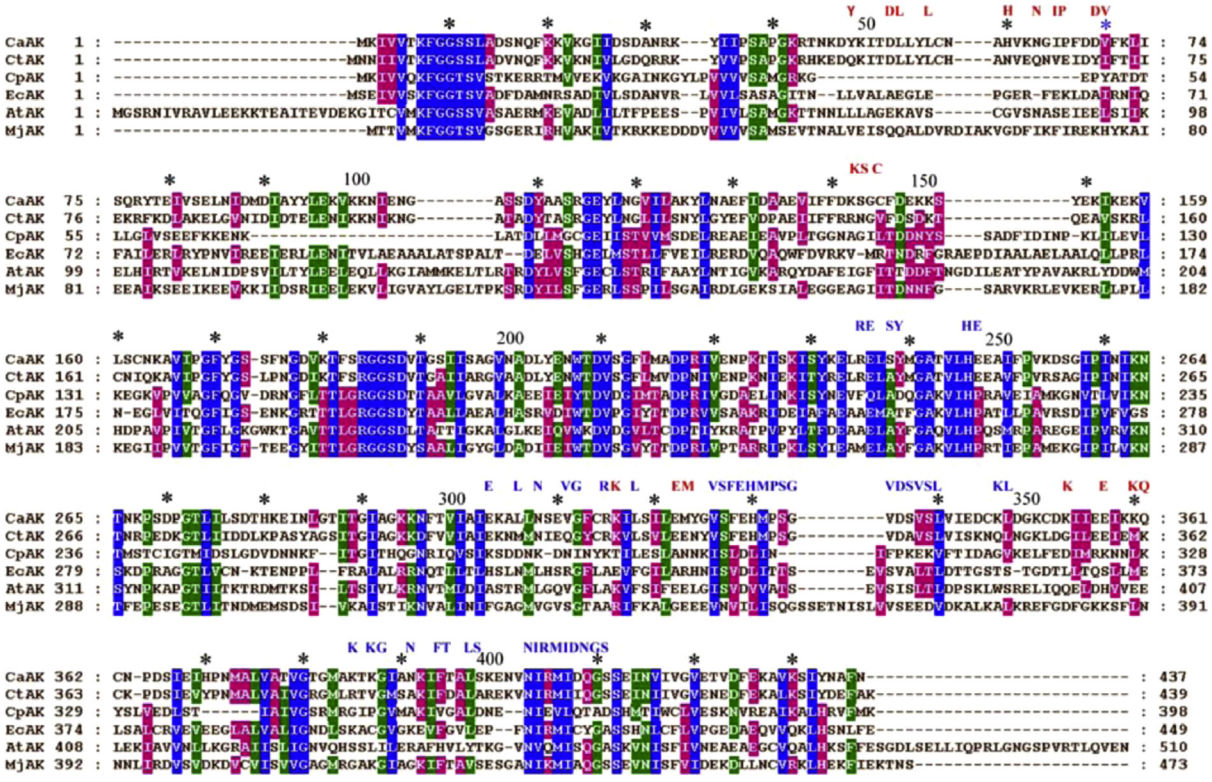

Fig. 1. Multiple sequence alignment against homologs. Aspartate kinases are identified as their abbreviation: *Ca*AK (sp Q97MC0; *C. acetobutyliucm*); *Ct*AK (sp Q891L5; *C. tetani*; 64.8% identity); *Cp*AK (sp Q8XJS6; *C. perfringens*; 25.6% identity); *Ec*AKIII (sp P08660; *E. coli*; 25.9% identity), *At*AK (sp Q9LYU8; *A. thaliana*; 28.4% identity) and *Mj*AK (sp Q57991; *M. jannashii*; 25.4% identity). Conservation of residues are shown in four layers, such as, fully (100%), highly (80%), partially (60%) and none with foreground shades in blue, green, pink and none colour respectively. The residues which are conserved in dimer and tetramer interaction are shown in blue and red letters at the top of the numbering line respectively. The alignment was generated using the program ClustalW [60]. (For interpretation of the references to colour in this figure legend, the reader is referred to the web version of this article.)

*Ca*AK represents a C-terminal regulatory domain that includes two small domains belonging to the ACT domain family (Pfam PF01842). ACT domains are ligand-binding domains that are found in a wide variety of regulated proteins [23,24].

The structural and biochemical studies of AKs from different organisms highlighted the molecular basis of the diversity of allosteric regulation and the many structural faces of AKs sensitive to the concerted inhibition [19,25]. Based on the crystallographic structures AKs are categorized into three classes. Class I contains the homo-dimeric enzymes from *E. coli*, *Methanococcus* jannaschii and *A. thaliana* with one catalytic domain and two ACT domains per monomer [26–28]. The dimerization is mediated by the association of the ACT domains. Class II contains to the hetero-tetrameric enzyme from *C. glutamicum* with one catalytic domain and two ACT domains per α-subunit and two ACT domains per β-subunit [29]. The oligomerization involves strong association of the catalytic domain of the α-subunits and the interaction of the ACT domains of α and β-subunits. Class III contains the homo-dimeric enzyme from *Synechocystis* with one catalytic domain and four ACT domains per monomer [9]. In this case, dimerization only involves the catalytic domain. However, there are many AKs from whole genomic database, but minimal crystallographic and biochemical data is available to demonstrate the regulatory principles of structural allostery. Here we report the crystallographic analysis of AK from *C. acetobutylicum* to a resolution of 3.0 Å in order to define the relationship between the assembly of AKs and the allosteric mechanism of AK, which may be relevant for industrial uses such as the development of effective lysine production strain.

2. Results and discussion

2.1. Overall structure of Ca*AK*

The structure of *Ca*AK was determined to 3 Å resolution by single wavelength anomalous dispersion (SAD) method. The crystals belong to the monoclinic space group $P2_1$ and forming a total of 576 kDa protein (12 monomers in asymmetric unit with each 48 kDa) which posed the problem of solving the constellation of 108 Se atoms (9 SeMet residues/monomer) in the asymmetric unit. The anomalous differences for the SeMet peak data used successfully to locate about 80% of Se atoms. The successful substructure solution presented here adds to the database of largest selenium substructures that has been determined to date [30]. Although the diffraction limit of the *Ca*AK crystals was relatively low (3 Å resolution). However, the resolution was compensated by the significant level of non-crystallographic symmetry (NCS) restraints, enabling refinement of the structure. The overall geometry of the model is of good quality, with 86% of the residues in the most favored regions and 14% in allowed regions of the Ramachandran map and model was refined to an R-factor of 20.7% (*R*free of 27.3%).

*Ca*AK monomer belongs to the class I type AKs which consists of one catalytic domain and two ACT domains (Fig. 1a) [25]. The superposition of complete chain of A on the other 11 chains yields root-mean-square deviation (r.m.s.d) between 0.68 Å and 1.36 Å, indicating that all 12 chains in the asymmetric unit of the *Ca*AK crystal are similar. The superposition of *Ca*AK dimer AB on the other dimers CD, EF, GH, IJ and KL in the asymmetric unit yield r.m.s.d's of

1.1 Å, 1.86 Å, 1.5 Å, 1.63 Å and 1.67 Å, respectively. The active biological unit of aspartate kinases is homodimeric which is formed between identical ACT domains from two neighboring subunits (Fig. 1b). ACT1 domains from chain A and B are arranged side-by-side with the creation of two equivalent effector binding sites at the interface. Similarly, ACT2 of one monomer interacts with the ACT2 of the other monomer. The homodimers are further associates into *Ca*AK tetramer (Fig. 1c). There were three tetramers of *Ca*AK observed in the asymmetric unit. A simultaneous least-squares superposition of the tetramer ABCD on to EFGH and IJKL tetramers results in alignment with r.m.s.d's of 2.4 and 2.9 Å, respectively. The three tetramers of *Ca*AK comprise six homodimers which exhibits essentially identical overall dimeric architecture.

The overall fold is similar to the other class I AKs although these shares very low sequence identity. Specifically, Fig. 2 compares *E. coli* aspartate kinase III (*Ec*AkIII-PDB 2J0X and 2J0W with r.m.s.d 2.2 Å and 3.8 Å, respectively; 25.9% sequence identity) [26], *A. thaliana* aspartate kinase (*At*AK-PDB 2CDQ; rmsd 3.0 Å; 26% sequence identity) [28], and *M. jannaschii* aspartate kinase (*Mj*AK-PDB 3C1N, 3C20 and 3C1M with rmsd 2.6 Å, 3.0 Å and 4.3 Å, respectively; 27.9% sequence identity) [27]. The N-terminal domain of *Ca*AK is considered to be the catalytic domain (AKα-residues 1–282) and belongs to the amino-acid kinase family [31] with a conserved eight-stranded β-sheet sandwiched between two layers of α-helices. The catalytic domain is further divided into the N-terminal lobe (residues 1–200 shown in purple) and the C-terminal lobe (residues 201–282 shown in brown color) [26–28]. The C-terminal domain is considered to be regulatory domain and two perpendicular ACT domains (ACT1 and ACT2 shown in pink and green respectively) having the architecture similar to the known class I AK structures. Previously, the ACT domain has been identified as modular regulatory unit associated with the control of variety of metabolic processes [9,32–34]. ACT1 (residues 295–372) has a βαββαβ topology similar to the typical ACT domain and was first identified in the structure of 3-phosphoglycerate dehydrogenase (PGDH; PDB 1YGY) [35]. ACT2 made up of C-terminal residues

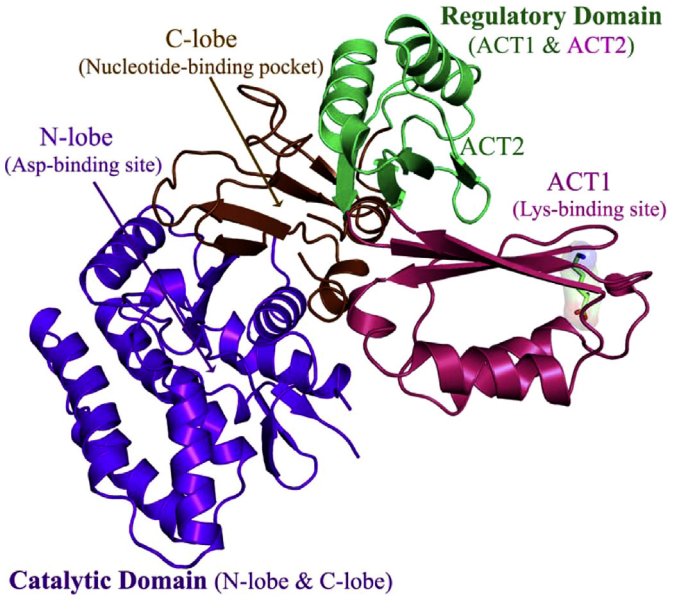

Fig. 2. Structure of *Ca*AK complexed with lysine. The N-lobe and C-lobe of catalytic domain are shown in purple and brown respectively. The substrates (aspartate and ADP) binding sites are shown. The regulatory domain contains ACT1 and ACT2 are shown in pink and green respectively. The effector binding site bound to lysine is represented in stick model with transparent surface. (For interpretation of the references to colour in this figure legend, the reader is referred to the web version of this article.)

372–437 has the topology βαββα and another β strand (residues 283–295) located before the ACT1 to complete the ACT domain architecture. This arrangement is first identified in the *At*AK [28]. The allosteric mechanisms associated with the ACT domains are generally linked to ligand binding to these domains elicits structural changes that alter the catalytic function at the active site located at the other region of the enzyme [36].

2.2. T-state homodimeric architecture of CaAK

The active biological unit of aspartate kinases is homodimeric which is formed between identical ACT domains from two neighboring subunits. ACT1 domains from chain A and B are arranged side-by-side with the creation of two equivalent effector binding sites at the interface. Similarly, ACT2 of one monomer interacts with the ACT2 of the other monomer. Thus, the entire regulatory domain consists of the four ACT domains making the core of 16 strands with eight-stranded antiparallel β-sheet with four helices on each side. The homodimeric arrangement of *Ca*AK closely resembles the T-state conformation of the AK structures (Fig. 3A and B). It was hypothesized from the crystal structures of *Ec*AKIII (PDB Ids 2J0X and 2J0W) that binding of lysine to the enzyme induces the conformational transition from the R-state to T-state (Fig. 3B and C). Close inspection of the electron density map reveals that two Lys molecules are bound at the ACT1 dimer interface of *Ca*AK (Fig. 7A) similar to the other lysine bound AK crystal structures further supporting a T-state conformation of our *Ca* AK structure. Further, the mean solvent accessible surface area (SASA) for the isolated *Ca* AK monomers and dimers are calculated to be 20,227 and 36,571 Å^2, respectively. The mean SASA between monomers and dimers is approximately 3880.6 and 7761 Å^2, respectively. These values are about 3% less when compared to the other structures of class I AKs (Table 3). The dimer interface present in the *Ca*AK is noteworthy for hydrophobic interactions that stabilize the homodimer including the interactions with the lysine bound between the ACT domains. The residues which are involved in dimeric interactions are shown in blue letters at the top of the sequence (Fig. 1). Dimerization of AK in solution has been reported [26–28,37] and has been also identified in the crystal state by X-ray crystallography. Further, nearly all class I AK crystal structures bound to effector molecules have been crystallized as a dimer of dimers. The tetramer interface is mainly mediated through the catalytic domain which is apparent across a crystallographic 2-fold axis of the T-state homodimeric *Ca*AK. Various solution studies were conducted to address the discrepancy in the quaternary structure of AK which revealed that the formation of the cooperative tetramer is possible upon effector binding [25,38].

2.3. Domain motion in CaAK

Despite the fact that the enzyme had been crystallized in the absence of lysine, the structure reveals lysine bound form of *Ca*AK which enable us to identify the key elements which are responsible for the large conformational changes associated with the inhibitor binding. The DynDom analysis clearly indentified the bending residues at the domain crossover regions (D208–L213 and E237–I250) in order to support the domain motion between the regulatory and catalytic domains of *Ca*AK (Fig. 4A and B). The analysis provides the rotation angle of monomers B, D, E, I as 7.3°; 8.2°; 7.3° and 3.7°, respectively whereas no rotational angle was detected for the monomers C, F, G, H, J, K and L when monomer A was used as the reference structure. Further rotational analysis on all combinations of monomers showed the rotational angle and the value lies between 4° to 8° between the monomers. The domain reorientation is mainly controlled by interaction between

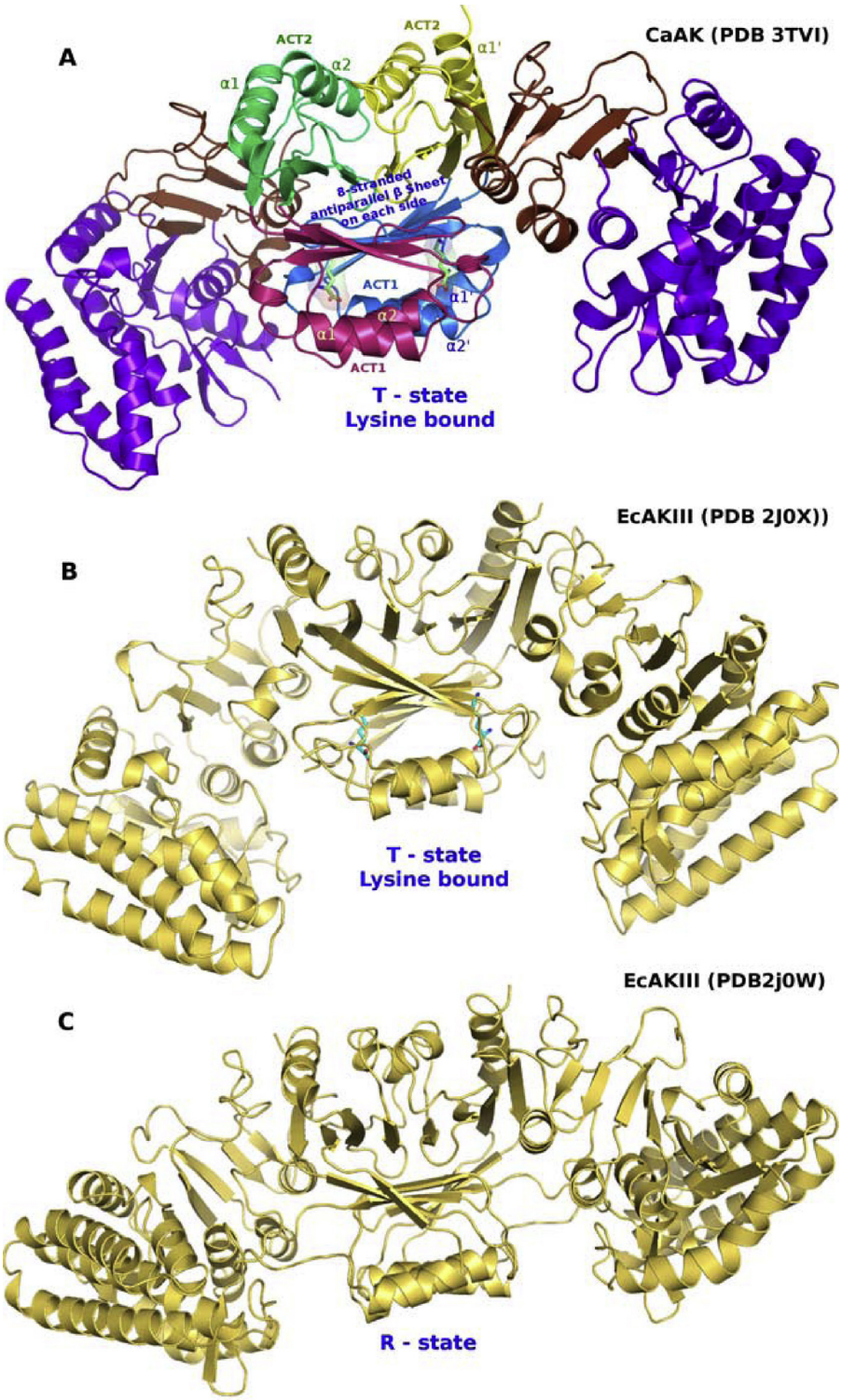

Fig. 3. Aspartate kinse homodimeric states: (A) lysine bound T-state homodimeric arrangement of *Ca*AK. Two lysine molecules (shown as stick representation) bound between the two ACT1 domains from different monomer (shown megenta and skyblue). ACT2 domains from different monomers (shown in green and pale yellow) stabilizing the dimer structure and transmitting the lysine binding signal to the catalytic domain. (B) Lysine bound T-state homodimeric arrangement of *Ec*AKIII homodimer (shown in yellow, PDB 2J0X); (C) R-state homodimeric arrangement of *Ec*AKIII homodimer (shown in yellow, PDB 2J0W). (For interpretation of the references to colour in this figure legend, the reader is referred to the web version of this article.)

the residues K232, R235, E236, S238, Y239, H246 and E247 of catalytic domain and E303, L306, N308, V335, D336 and S337 of regulatory domains. The varied interaction is induced by either lysine binding at the homodimeric interface or nucleotide binding/release at the domain crossover regions. In order to support this observation, the relative reorientation of the domains is observed in different *Mj*AK complex structures (PDB Ids 3C1N, 3C20 and 3C1M). The rotational angle varies between 6.3° and 18.9° and demonstrates the inhibitor, substrate and cofactor binding to *mj*AK induces the conformational changes between the domains. Both

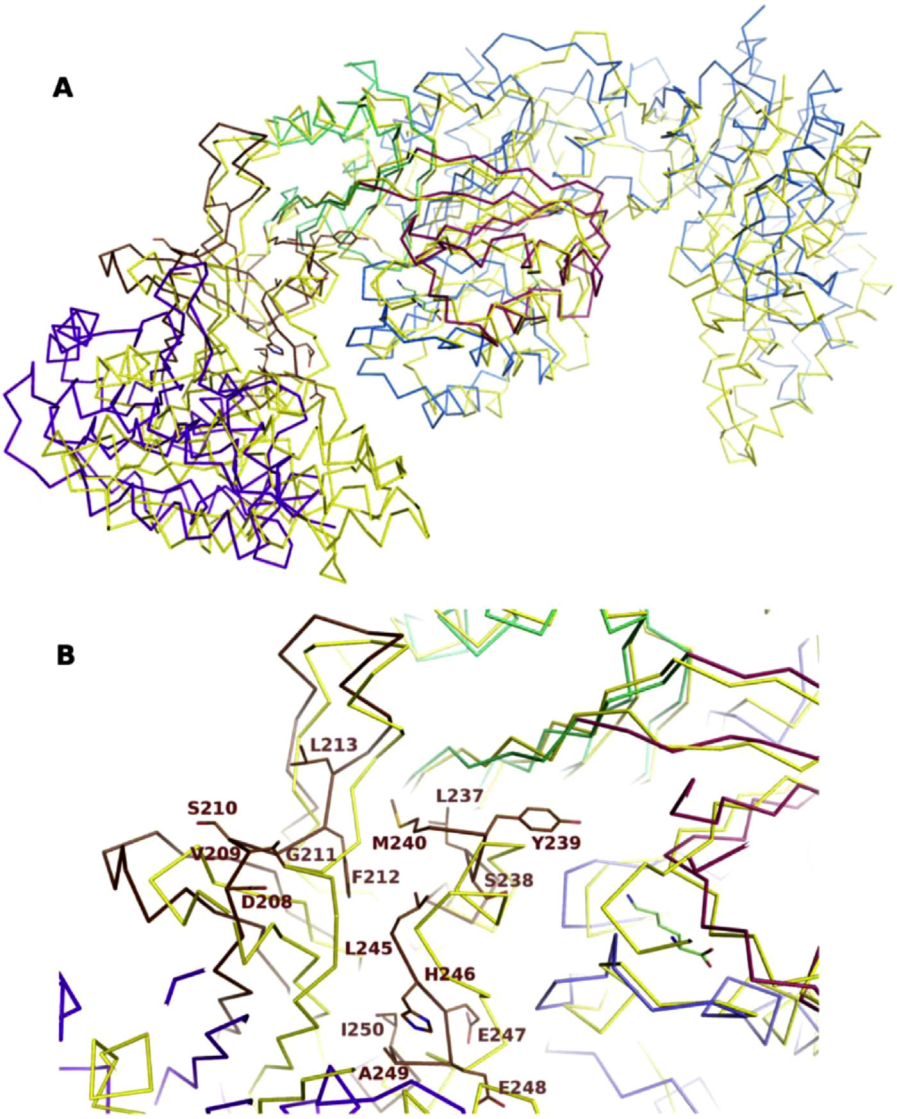

Fig. 4. Domain motion in aspartate kinase: (A) superposition of T-state *Ec*AKIII homodimer (shown in yellow, PDB 2J0X) on the *Ca*AK homodimer represents the more open conformation due to increased relative re-orientation of catalytic domains. (B) Zoom view of the domain crossover regions and corresponding residues. (For interpretation of the references to colour in this figure legend, the reader is referred to the web version of this article.)

the *Ca*AK and *Mj*AK structures have shortened latch loop regions (*Ca*AK: E343–D348 and *Mj*AK: S366–V370) and do not appear to play a role in conformational arrangements. In contrast, the crystal structures of *Ec*AKIII solved in both R- and T-state conformation (PDB Ids 2J0X and 2J0W) demonstrated the largest rotation (∼36.3°) between the catalytic and regulatory domain. The critical latch loop (D354–T364) leading to the transition from R- to T-state and tetramer formation that undergoes major rotational rearrangements. The latch loop is well conserved in the structure of *At*AK (D387–I397) appears to play a role in conformational rearrangements and tetermer formation similar to *Ec*AKIII. The superposition of four ACT domains of *Ca*AK dimer on the corresponding four ACT domains of dimeric structures of *Ec*AKIII (PDB 2J0X and 2J0W with rmsd of 1.3 Å and 1.5 Å, respectively), *At*AK (PDB 2CDQ with rmsd of 4 Å), *Mj*AK (PDB 3 C1 M, 3 C1 N and 3C20 with rmsd of 2 Å; 1.9 Å and 1.8 Å, respectively) revealed that ACT domains adopt a similar conformation. However, the domain reorientation is observed in comparison with *Ec*AKIII, *At* AK and *Mj*AK homodimers. Fig. 3B represents the superposition of regulatory domains of *Ca*AK homodimer on the *Ec*AKIII T-state structure (2J0X). The regulatory domains were aligned with low rmsd (1.3 Å). In contrast, the catalytic domains of monomer A and B of *Ca*AK were rotated outwards with an angle of 15.4° and 22.9° with respect to dimer of *Ec*AKIII T-state structure (Fig. 4A and B). This supports the observation that the increased open T-state conformation which is mainly due to the catalytic domain reorientation which is linked to the catalytic mechanism of the enzyme.

2.4. Tetramer formation in CaAK

The rotational rearrangement of catalytic domains of *Ca*AK ultimately induced to form a compact tetramer (Fig. 5A) which is unique among any other tetramer observed in class I AKs. Fig. 6 represents the tetrameric views observed in the structures of *Ec*AKIII, *At*AK and *Mj*AK. The various snapshots of AK tetramers show the decrease in size of the central cavity due to an increase in rotational angle between the catalytic domains leading to more

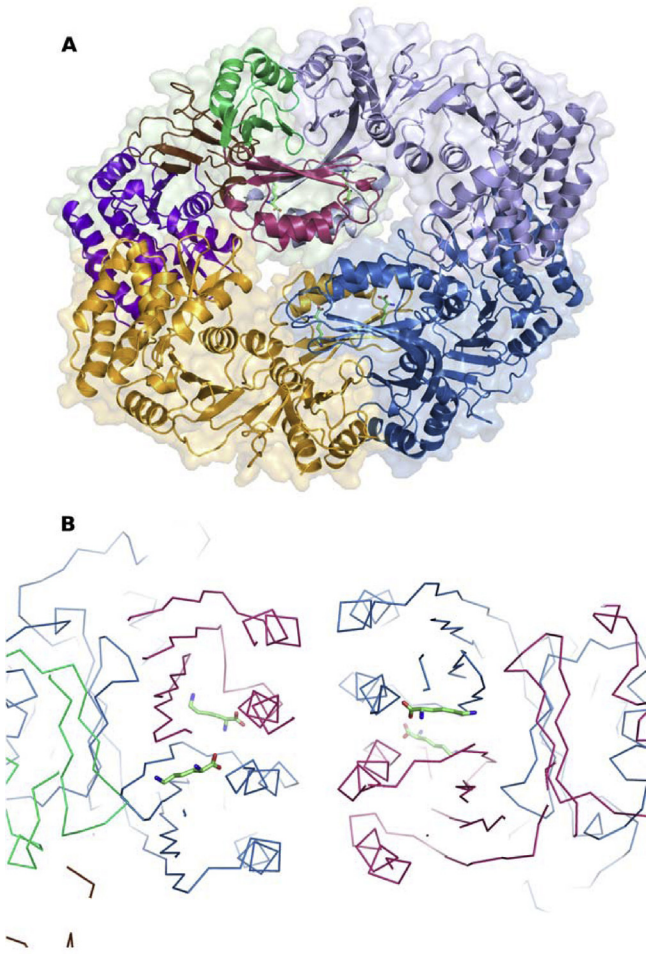

Fig. 5. Aspartate kinase Tetramer. (A) Cartoon representation of the compact tetramer formed between the two homodimers of *Ca*AK. Surface representation is also shown. (B) Zoom view of the interaction of four helices of the ACT1-ACT1 domains from the different homodimers are shown.

open conformations. Interestingly, the *Ca*AK dimers of dimers increased number of interactions with regulatory domain (ACT domains – four helices each side – Fig. 5B) in addition to the regular interactions at either side of the catalytic domains. The residues which are involved in tetrameric formation are shown in red letters at the top of the numbering line (Fig. 1). The central cavity is completely closed in *Ca*AK structure which increases in tetrameric buried surface area (BSA). BSA is about 4–5% in all the class I AKs whereas in the *Ca*AK tetramer it is about 8% (Table 3). The significance of the dimer to tetramer transition observed in *Ca*AK structure is also valid biochemically. Firstly, despite the low value of this interface, solution measurements indicate that this binding affinity is strong enough to sustain tetramer formation. Secondly, given the fact that the similar tetrameric interactions occur four times in different crystallographic environments including in the structure of *Ca*AK with different snapshots supports that the tetramer formation is biochemically relavant phenamenon (Fig. 6). Thirdly, the interactions obesrved between the ACT domains (Fig. 5B) of *Ca*AK homodimers were not obereved in any known AK structures. Finally, the tetrameric view of the *Ec*AKIII represents the most open tetrameric form and the structures *Mj*AK (3 C1 M) and *Ca*AK are the most compact tetrameric structures. Fig. 6F represents the superposition of the tetrameric views of *Mj*AK on the *Ca*AK (shown in pink) reveals that *Ca*AK tetramers are most compact ever observed and which is unique among other tetrameric organization of the class I AK structures. The transformation of the open form to the closed form tetramer observed in class I AK structures provide the evidence that they are genuine biochemical entities.

2.5. Network of residues involved in catalytic and regulatory roles

2.5.1. Lysine binding site

The crystallographic structures of AK's reveal that the different organizations in ACT domains lead to a great variety of control allowing allosteric inhibition by lysine or threonine [9,28]. The residues from monomer A (N308, G312, C314, F313, S333, G334, G335, S336) and monomer B (S327, F328 and E329) are interacting with lysine in the crystal structure of *Ca*AK (Fig. 7B). Lysine–protein interactions pattern more similar in the lysine bound structures of *Ec*AKIII (PDB 2J0X) and *At*AK (PDB 2CDK) than the threonine bound structure *Mj*AK (PDB ID 3C1N). In the structure of *Ec*AKIII, the residues M318, S321, G323, F324, L325, T344, S345, G346 from monomer A and residues S338, V339, D340 from monomer B are involved in lysine binding (Fig. 7C). The mutational analysis of *Ec*AKIII detected two amino acid residue regions (318–325 and 345–352) that may be important in feedback inhibition in *Ec*AKIII [39]. On comparison essential/conserved residues between the structures of *Ca*AK and *Ec*AKIII reveals that the residue C314 might play an important role in binding the lysine in *Ca*AK structure. Recently, *in silico* studies combined with co-evolutionary analysis on *Ec*AKIII further confirmed the previous studies and helped to identify the network of residues involved in allosteric regulation [40].

2.5.2. Asp binding site

The multiple sequence alignment of *Ca*AK against class I AKs suggests that the catalytic activity and aspartate binding residues are fully conserved. Previous site directed mutagenesis and crystallographic studies of *Ec*AKIII identified two residues, K8 and D202, that appear to play roles in the enzymatic activity while residues E119 and R198 are involved in the binding of amino acid substrate, having interactions with the α-NH_3^+ and α-COO^- groups of aspartate, respectively [41]. Interestingly, the multiple sequence alignment of *Ca*AK on *Ec*AKIII suggests that corresponding residues K7 (K8 of AKIII), D188 (D202 of AKIII), E116 (E119 of AKIII) and R184 (R198 of AKIII) are fully conserved (Fig. 1) in *Ca*AK. The aspartate binding environment of *Ca*AK is homologous to other class I AKs.

2.5.3. Nucleotide binding site

Most of the residues at the domain crossover regions (W208–G213 and E237–I250) are also conserved (Fig. 4B). In the crystal structure of *Mj*AK, the residues D239 and R241 are involved in binding to nucleotide. The sequence alignment shows that the corresponding residues D216 and R218 are conserved in *Ca*AK (Fig. 1). In the structure of *Ca*AK the residues at nucleotide binding region shows disorder. The residues from Y239 to L245 are not visible in the electron density map for the chains A, C, F, G, I, K and L whereas for the chains B, D, H and J these residues are visible with elevated temperature factors without the side chains for some of the residues. This observation suggests that the nucleotide binding to *Ca*AK will be similar to that of *Mj*AK. The main differences between all class I AK structures are with relative orientation of the sub-domains and variable length of the latch loop between the catalytic and regulatory domains. The structural differences are linked to differentiate the end-product (lysine/threonine) sensitiveness of AKs [27].

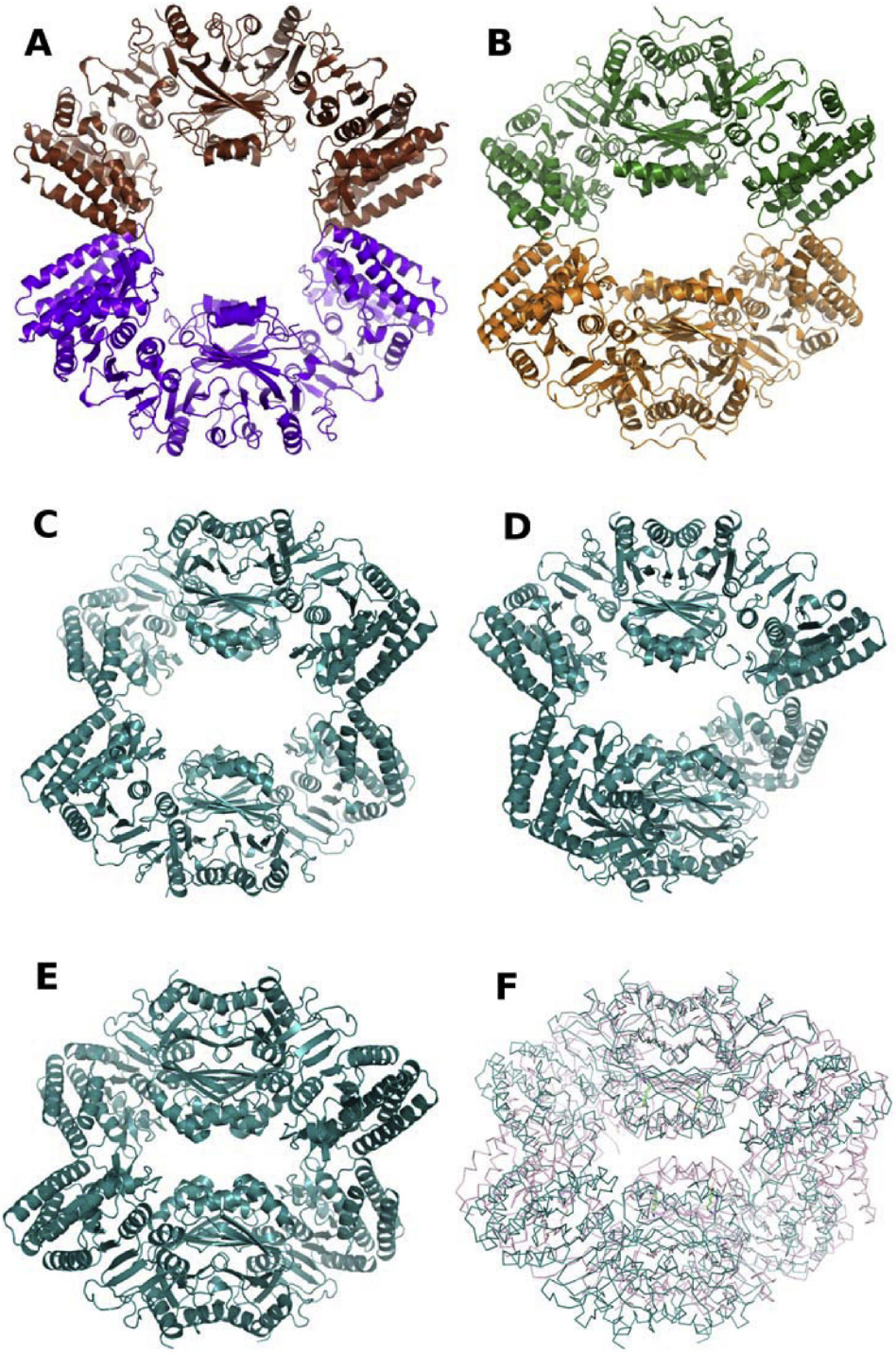

Fig. 6. Aspartate kinase tetrameric states. (A) *Ec*AKIII (PDB 2J0X), (B) *At*AK (PDB 2CDQ), (C) *Mj*AK (PDB 3C1N), (D) *Mj*AK (PDB 3C20), (E) *Mj*AK (PDB 3C20), (F) Superposition of the most compact tetrameric forms are shown: *Mj*AK (PDB 3C20) on the *Ca*AK (shown in pink). (For interpretation of the references to colour in this figure legend, the reader is referred to the web version of this article.)

2.6. Allosteric regulation and biotechnological relevance of the enzyme

Aspartate kinase in an allosteric enzyme has a wide applications in biotechnological industry and mainly responsible for the biosynthesis of amino acids. The efficiency of biosynthesis is largely depends upon quality of strains used in microbial fermentation. The understanding of the metabolic pathways of lysine biosynthesis and regulation through metabolic engineering helps to the effective strain development. The enzymatic action and mechanism of inhibition of aspartate kinase is well understood through large number of crystallographic and biochemical analysis. However, continued efforts have been made to understand the mechanism and regulation of aspartate kinase from suitable organism to define the successful construction of industrially producing strains. In the aspartate kinase, the binding of lysine to the regulatory domain triggers the structural rearrangements for formation of tetrameriztion of the biological homodimers (Fig. 5). Concurrently, the allosteric transition of the

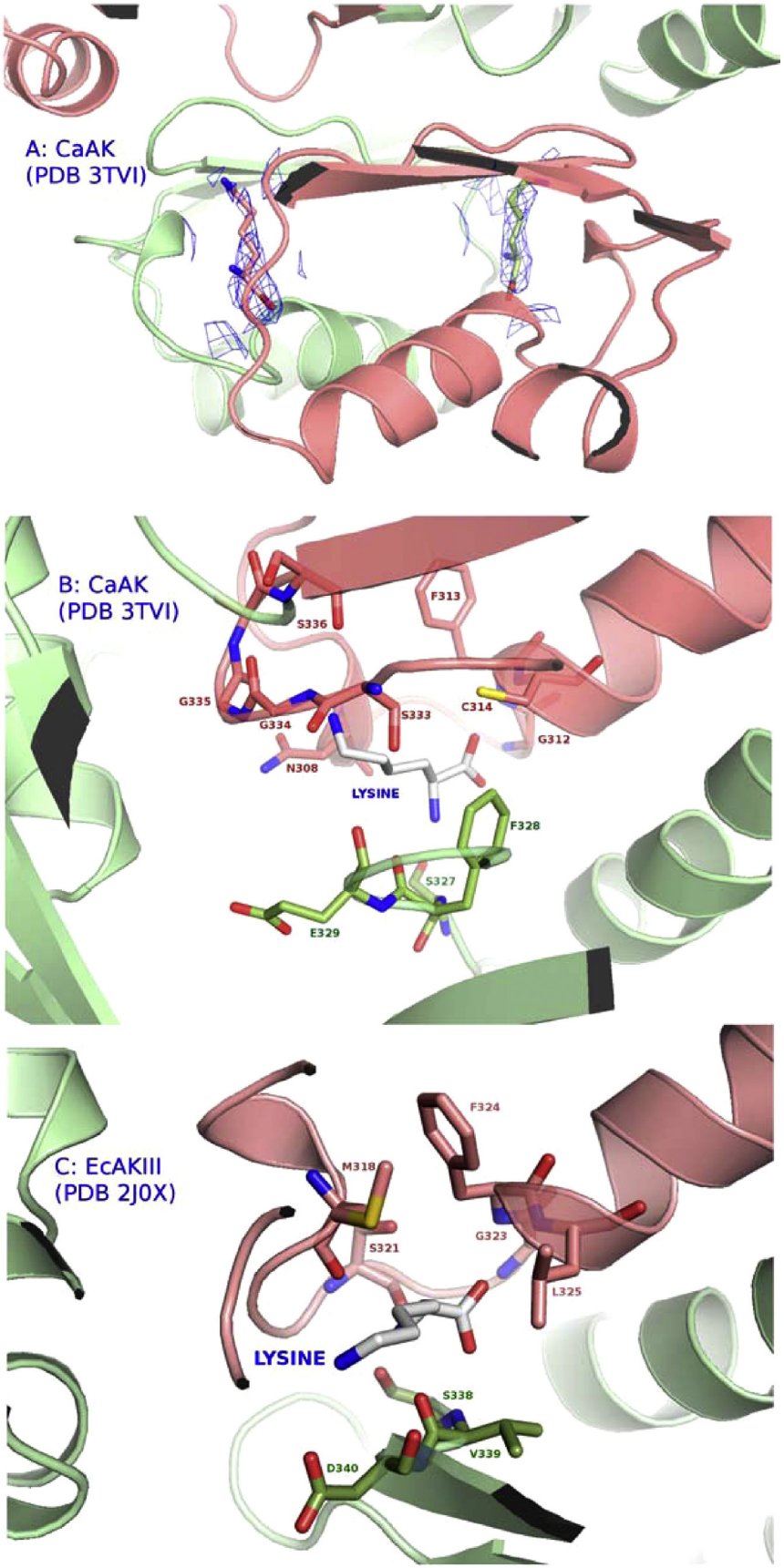

Fig. 7. Lysine binding site: (A) electron density representation contoured at 1σ level for the lysine molecules bound between the two ACT1 domains from different monomers. (B, C) Zoom view of the lysine binding region in *Ca*AK and *Ec*AKIII (PDB 2J0X) structures (corresponding residues are labelled).

catalytic domain leads to blocking of the nucleotide binding site and eventually loss of enzymatic activity. In *Ca*AK, the mechanism of inhibition follows the similar fashion when compare to the other class I AK enzymes. Mainly, most of the structural elements which are implicated in probing the catalytic, substrate-binding and allosteric mechanisms are conserved. Secondly, the way of binding of lysine molecules at the interface of the two ACT1 domains from different monomers provides to identify the residues which are implicated in lysine interactions. This structural observation can be tested by studying inhibition profile of lysine in *Ca*AK. Further, site-directed mutational analysis of these residues makes it possible to engineer the lysine binding site. This eventually helps to manipulating the biosynthesis of amino acid to increase the amino acid content and nutritive value in crops. Recently, much work has been done to metabolically engineered crops and grains with enhanced amino acid levels [42,43]. Thirdly, the mechanism of structural transition to tetramer assembly is similar way to the other three different crystallographic environments. However, the tetramer configuration of *Ca*AK is totally different than the other known AK structures. The improved understanding plant amino acid biosynthesis pathways potentially helps to design strategies employed for metabolic engineering. Finally, most of the residues which are implicated in probing the catalytic, substrate-binding and allosteric mechanisms are also conserved in pathogenic *Ct*AK and *Cp*AK. Therefore, the structure we reported here will provide useful information for drug design targeting on pathogenic AKs.

3. Conclusion

AK is a key enzyme controlling the biosynthesis of lysine. The allosteric regulation of AK represents a typical mechanism of metabolic control of strong rigid node, i.e., node is tightly controlled at one of its branches by a combination of feedback control and enzyme activation by metabolites from a competing branch. The specific enzyme (AK) is feedback inhibited by its end product either by lysine or threonine and activated by metabolite from a competing branch (Asp). The presence of lysine in the structure of *Ca*AK (despite lysine is not part of crystallization buffer) speculate that *Ca*AK is more sensitive to be inhibited by lysine than the threonine. The crystal structure of *Ca*AK provides a unique view of compact cooperative tetrameric oligomers which yield insights into the molecular determinants for catalytic and regulatory roles of the widespread and biotechnologically important aspartate kinase enzymes.

4. Materials and methods

4.1. Protein purification and crystallization

Purified native and selenomethionine-substituted (SeMet) *Ca*AK protein was obtained from the New York SGX Research Center for Structural Genomics (PSI TargetTrack: NYSGXRC-6204b). The protein with selenomethionine labeling was expressed in *E. coli* high yield (HY) media and purified by standard NYSGXRC protocol [43–46]. The HY media is prepared using following procedure. To a 2 L baffled flask containing 950 ml autoclaved Milli-Q water add one packet of M9 salts, 10 mL of mineral supplement, 1 mL of vitamin supplement, 1 mL of antibiotic (kanamycin −30 mg/mL solution) and 10 mL 50% glycerol. Mix flask and allow salts to go in to solution before using. Briefly, a full-length cDNA fragment of aspartate kinase (GenBank AE001437) was amplified by polymerase chain reaction (PCR) from *C. acetobutylicum* (strain ATCC 824) genomic DNA using forward (AAAATCGTAGTAACAAAGTTTGG) and reverse (CATTAAATGCATTGTATATGGATTTAACAGC) primers. The PCR product was cloned into a vector pET modified for topoisomerase directed cloning (Invitrogen) and designed to express the protein of interest followed by a C-terminal hexa-histidine tag then was transformed into TOP10 cells. The resulting clone was grown by adding 500 mL of Luria–Bertani (LB) medium containing 500 μL of 30 mg/mL kanamycin, 25 mL of 10% glucose, and a small amount of transformed cell glycerol stock scraping to a 2 L baffled flask at 30 °C with overnight shaking (250 rpm). 10 mL of the resulting culture was added to each of six flasks containing similar culture medium for large scale expression. The cultures were subjected to shaking under similar conditions until the OD_{595} reached to the range of ~0.8. The protein expression was induced by adding 200 μL of 1 M isopropyl-D-thiogalactopyronoside (IPTG). After overnight vigorous shaking (250 rpm, 21 °C), the cells were pelleted by centrifugation (in 1 L spin bottles; at 6500 rpm for 10 min). The pellets were collected into 50 mL conical tubes and re-suspended in a lysis buffer (35 mL/10 g), 50 μL of protease inhibitor cocktail tablet (Sigma and 5 μL of benzonase (Novagen). The cells were lysed by repeated sonication (with intervals of cooling) followed by centrifugation (38,900 *g* for 30 min). The filtrate was then immobilized on Ni-NTA-agarose resin (Qiagen), placed on a drip column and washed with 25 mL buffer-A (50 mM Tris–HCl pH 7.8, 500 mM NaCl, 10 mM imidazole, 10 mM methionine, and 10% glycerol). The protein was eluted into an Amicon concentrator (Millipore) with 15 mL of buffer-A containing 500 mM imidazole. The eluted protein was concentrated to 6 mL and loaded onto a gel filtration column (Superdex 200, Pharmacia). The fractions were pooled, concentrated to 13.5 mg/mL and stored in 10 mM hepes pH7.5, 150 mM NaCl, 10 mM methionine, 5 mM dithiothreitol (DTT), 10% glycerol. Similarly, seleno-methionine labeled protein was produced, purified and concentrated to 9.3 mg/mL. The clone is available through DNASU.org as CaCD00423555.

Initial crystallization screening was performed on both Native and SeMet-labelled proteins using the Hampton index screen (Hampton Research, CA, USA). Microcrystals were observed from several conditions and optimization screens were applied adjacent to condition #71 (25% PEG 3350 and 100 mM Tris pH 6.5, 200 mM NaCl), which provided the best crystals. Fan shaped crystals were obtained for SeMet-labelled protein in an optimized condition containing 13% PEG 3350 and 100 mM Tris HCl pH 6.5. Droplets comprising 1.3 μL of protein plus 1.3 μL reservoir solution was

Table 1
Crystallographic data-collection statistics.

X-ray source	NSLS X29 Beamline
Wavelength (Å)	0.9792
Space Group	$P2_1$
Cell parameters (Å, °)	a = 109; b = 274.2, c = 114 α = 90, β = 113.7, γ = 90
No. of molecules in an asymmetric unit	12
Resolution range (Å)	20–3.0
B-factor Wilson plot (Å^2)	70
Mosaicity range (°)	0.6–0.9
Total Reflections	724, 519
Unique Reflections	217, 894
Completeness (%)[a,b]	89.9 (79.7)
Redundancy	3.0 (2.8)
Mean I/σ (I)	14.0 (2.0)
Rmerge(%)[b,c]	8.5 (72.8)
SHELXD[d]: Data used (Å)	20–3.8
Correlation coefficient CC all/weak	45.69/32.02
Combined figure of merit (CFOM)	60.1
PAT figure of merit (FOM)	2.94
Number of Se atoms located	92 out of 108
ADDSOLVE FOM[d]	0.33
RESOLVE FOM with 12-fold NCS[d]	0.53

[a] Data completeness treats Bijvoët mates independently.
[b] Statistics for the highest resolution bin (1.9–1.93 Å) are given in parentheses.
[c] $R_{\text{merge}} = \sum_{hkl} \sum_i | I(hkl)_i | - < I(hkl) > | / \sum_{hkl} \sum_i < I(hkl)_i >$.
[d] Substructure determination parameters are from SHELXD, ADDSOLVE and RESOLVE.

Table 2
Refinement and ramachandran plot statistics.

Resolution range (Å)	20–3
Reflections used for refinement (all)	104, 822
Reflections used for *R*free	5511
*R*cryst(%)[a]	20.6
*R*free (%)	27.3
r.m.s.d. bond lengths (Å)	0.006
r.m.s.d. bond angles (°)	1.057
Favored region (%)	86 (3964)
Additional allowed region (% and number of residues)	14 (645)
Generously allowed regions (% and number of residues)	0.0
Outliers (%)	0.0

[a] $R_{cryst} = \sum_{hkl} || F_o(hkl) | - k | F_c(hkl) || / \sum_{hkl} | F_o(hkl) |$, where F_o and F_c are observed and calculated structure factors.

equilibrated against 500 μL in reservoir solution. Consequently, further work including crystallization trials with different additives and streak seeding methods were undertaken with the aim of obtaining better quality crystals. However, none of these trials improved the crystal quality.

4.2. X-ray data collection and processing

The freshly prepared crystals were very fragile and became rubbery after several days. These crystals diffracted poorly (to 4 Å resolution) at beamline X3A and at 3.6 Å resolution at beamline X29 of the national synchrotron light source (NSLS), Brookhaven National Laboratory, New York. Optimization of cryo-protection conditions helped in improving the diffraction properties of these crystals and an X-ray dataset collected to 3.0 Å resolution at the X29 beamline. Prior to data collection, a large crystal with a maximum dimension was placed into mother liquor containing 10%, 20% and 30% glycerol for 10–15 s intervals, followed by immediate flash cooling to 100 K in a liquid nitrogen stream. Single-wavelength anomalous dispersion (SAD) data were collected at the Se peak wavelength (0.9792 Å). The radiation damage affected the quality of dataset collected at inflection and remote wavelengths. The data were integrated with the program HKL2000 and scaled with SCALEPACK [47]. Data collection statistics are shown in Table 1.

4.3. Structure determination and refinement

The crystals belong to the monoclinic space group $P2_1$ with unit cell parameters $a = 109$ Å, $b = 274.2$ Å, $c = 114$ Å, $\beta = 113.7°$. The calculation of the Matthew's coefficient based on the molecular weight of 48,030 Da results in a V_M of 2.7 Å^3 Da^{-1} and a solvent content of 54%, which corresponds to the presence of twelve molecules in the asymmetric unit [48]. The anomalous differences for the peak data were used to successfully locate 87 out of 108 selenium anomalous scatterers with the structure solving package SHELXD [49]. The correlation coefficient, CC, was all/weak: 45.69/32.02 and Patterson figure of merit, PATFOM: 2.94. The selenium sites were refined along with additional 5 selenium sites identified and initial phases were calculated to overall figure of merit of 0.33 with the program ADDSOLVE [50]. Further, phases were improved to a figure of merit of 0.53 using solvent flattening and twelve-fold non-crystallographic symmetric averaging (NCS) in RESOLVE [51] which yielded a partial model. The electron density map was further improved by using single wavelength (Se peak) data as the starting point in the MRSAD anomalous dispersion protocol of the auto-rickshaw software pipeline which improved the model substantially [52]. Several rounds of manual model building with Coot [53] and refinement with the program REFMAC5 [54,55] were carried out. The final model ($R = 0.207$, Rfree $= 0.273$) contains 5352 residues from 12 molecules in asymmetric unit (446aa × 12mols) along with six lysine and seven aspartate molecules. The model quality was monitored using PROCHECK [56]. The coordinates and structure factors were deposited in the RCSB Protein Data Bank

Table 3
Surface area composition between the class I ak structures.

Enzyme (PDB) chains	Tetramer surface area (buried area)	Dimer surface area (buried area)	Monomer surface area (buried area)	Homodimeric interface area		Same side monomers interface 1		Opposite sidemonomers interface 2	
				Area	% of surface	Area	% of surface	Area	% of surface
*Ca*AK (3TVI) ABCD	70,000 (10,830)	36,390 (4020)	19,906.0 (2702.3) 20,510.1 (2704.2)	2020.2	19	558.1	5	174.4	2
		36,370 (4040)	20,267.0 (2752.7) 20,147.9 (2671.6)	2011.3	19	516.6	5	134.8	1
*Ca*AK (3TVI) EFGH	69,400 (11,060)	36,230 (3710)	20,103.7 (2712.0) 20,415.3 (2751.9)	1853.7	17	632.6	6	359.3	3%
		36,940 (3580)	20,385.9 (2845.7) 19,550.4 (2748.6)	1788.6	16	564.1	5	330.7	3
*Ca*AK (3TVI) IJKL	70,629 (10,810)	37,020 (4010)	20,158.3 (2718.3) 20,251.1 (2644.6)	2005.6	19	546.3	5	209.5	2
		36,480 (3920)	20,698 (2744.9) 20,333.8 (2704.2)	1962.4	18	529.9	5	152.2	2
*Mj*AK (3C1M) ABCD	68,760 (13,490)	35,390 (5710)	20,689.9 (3382.5) 20,458.5 (3349.9)	2856.3	21	538.4	4	None	None
		35,460 (5690)	20,576.3 (3394.8) 20,524.9 (3362.9)	2844.0	21	505.8	4	None	None
*Mj*AK (3C1N) ABCD	70,860.9 (13,737.9)	36,010 (5810)	20,954.7 (3434.8) 20,867.5 (3404.9)	2934.7	21	529.4	4	None	None
		36,910 (5870)	21,120.1 (3434.1) 21,656.5 (3464.1)	2905.4	21	499.4	4	None	None
*Mj*AK (3C20) AB	69,814.8 (14,708.8)	35,900 (6360)	21,190.7 (3686.7) 21,071.1 (3667.7)	3178.9	21	498.3	3	None	None
*Ec*AK (2J0X) AB	67,320 (13,500.7)	34,800 (5610)	20,154.2 (3375.2) 20,254.7 (3375.2)	2804	21	571.1	4	None	None
*At*AK (2CDQ) AB	74,060 (13,990)	38,070 (5960)	21,969.6 (3497.7) 22,054.9 (3496.4)	2979.2	21	518.8	4	None	None

under accession code 3TVI. Tables 1 and 2 details our data collection and refinement statistics. Structural presentation was generated using the program PyMol. The solvent-accessible surface of monomers, dimer and tetramers as well as their interacting interface was analyzed by PISA server [57]. Protein domain motions were analyzed by using the DynDom server [58].

Acknowledgements

We thank the beamline staff (Mike Sullivan, John Toomey, and Don Abel) of the Center for Synchrotron Biosciences. We wish to thank Jacqueline Freeman for cloning, Kevin Bain for protein expression, Davin Henderson for protein purification, and Elena Fedorova for initial technical assistance with robotic crystallization screening. This research is supported by the Biomedical Technology Resource Program of the National Institute for Biomedical Imaging and Bioengineering under P41-EB-01979 and P30-EB-09998 and a Protein Structure Initiative grant to the NYSGXRC funded by the National Institute for General Medical Sciences under U54-GM-74945. We thank Dr. J. Michael Sauder (Lilly Biotechnology Center, 10300 Campus Point Dr, San Diego, CA, USA) and Dr. Ranaud Dumas, (Laboratoire de Physiologie Cellulaire & Végétale, CEA, CNRS, INRA, UJF, UMR 5168, 38054 Grenoble, France) for critical reading and comments on this manuscript.

References

[1] G. Jander, V. Joshi, Recent progress in deciphering the biosynthesis of aspartate-derived amino acids in plants, Mol. Plant 3 (2010) 54–65.
[2] G.N. Cohen, The common pathway to lysine, methionine, and threonine, in: J.E. Davies, K.M. Hermann, R.L. Somerville (Eds.), Amino Acids: Biosynthesis and Genetic Regulation, Addision-Wesly Publishing Co., Reading, MA, 1983, pp. 147–171.
[3] G. Curien, S. Ravanel, M. Robert, R. Dumas, Identification of six novel allosteric effectors of *Arabidopsis thaliana* aspartate kinase-homoserine dehydrogenase isoforms. Physiological context sets the specificity, J. Biol. Chem. 280 (2005) 41178–41183.
[4] R.E. Viola, The central enzymes of the aspartate family of amino acid biosynthesis, Acc. Chem. Res. 34 (2001) 339–349.
[5] A. Rosner, H. Paulus, Regulation of aspartokinase in *Bacillus subtilis*. The separation and properties of two isofunctional enzymes, J. Biol. Chem. 246 (1971) 2965–2971.
[6] L.M. Graves, R.L. Switzer Aspartokinase III, A new isozyme in *Bacillus subtilis* 168, J. Bacteriol. 172 (1990) 218–223.
[7] M. Nishiyama, M. Kukimoto, T. Beppu, S. Horinouchi, An operon encoding aspartokinase and purine phosphoribosyltransferase in Thermus flavus, Microbiology (Reading, Engl) 141 (Pt 5) (1995) 1211–1219.
[8] J. Kalinowski, J. Cremer, B. Bachmann, L. Eggeling, H. Sahm, A. Pühler, Genetic and biochemical analysis of the aspartokinase from *Corynebacterium glutamicum*, Mol. Microbiol. 5 (1991) 1197–1204.
[9] A.Y. Robin, D. Cobessi, G. Curien, M. Robert-Genthon, J.L. Ferrer, R. Dumas, A new mode of dimerization of allosteric enzymes with ACT domains revealed by the crystal structure of the aspartate kinase from *Cyanobacteria*, J. Mol. Biol. 399 (2010) 283–293.
[10] L. Schuldt, R. Suchowersky, K. Veith, J. Mueller-Dieckmann, M.S. Weiss, Cloning, expression, purification, crystallization and preliminary X-ray diffraction analysis of the regulatory domain of aspartokinase (Rv3709c) from *Mycobacterium tuberculosis*, Acta Crystallogr. Sect. F Struct. Biol. Cryst. Commun. 67 (2011) 380–385.
[11] H. Nishida, I. Narumi, Phylogenetic and disruption analyses of aspartate kinase of *Deinococcus radiodurans*, Biosci. Biotechnol. Biochem. 71 (2007) 1015–1020.
[12] G. Curien, O. Bastien, M. Robert-Genthon, A. Cornish-Bowden, M.L. Cárdenas, R. Dumas, Understanding the regulation of aspartate metabolism using a model based on measured kinetic parameters, Mol. Syst. Biol. 5 (2009) 271.
[13] X. Chen, S. Schauder, N. Potier, A. Van Dorsselaer, I. Pelczer, B.L. Bassler, et al., Structural identification of a bacterial quorum-sensing signal containing boron, Nature 415 (2002) 545–549.
[14] G.J. Lyon, R.P. Novick, Peptide signaling in *Staphylococcus aureus* and other Gram-positive bacteria, Peptides 25 (2004) 1389–1403.
[15] K. Ragkousi, P. Eichenberger, C. van Ooij, P. Setlow, Identification of a new gene essential for germination of *Bacillus subtilis* spores with Ca^{2+} -dipicolinate, J. Bacteriol. 185 (2003) 2315–2329.
[16] C.J. Roberts, E.U. Selker, Mutations affecting the biosynthesis of S-adenosyl-methionine cause reduction of DNA methylation in *Neurospora crassa*, Nucleic Acids Res. 23 (1995) 4818–4826.
[17] J. Van Heijenoort, Recent advances in the formation of the bacterial peptidoglycan monomer unit, Nat. Prod. Rep. 18 (2001) 503–519.
[18] J. Kalinowski, B. Bathe, D. Bartels, N. Bischoff, M. Bott, A. Burkovski, et al., The complete *Corynebacterium glutamicum* ATCC 13032 genome sequence and its impact on the production of L-aspartate-derived amino acids and vitamins, J. Biotechnol. 104 (2003) 5–25.
[19] G. Curien, V. Biou, C. Mas-Droux, M. Robert-Genthon, J.-L. Ferrer, R. Dumas, Amino acid biosynthesis: new architectures in allosteric enzymes, Plant Physiol. Biochem. 46 (2008) 325–339.
[20] J. Lee, H. Yun, A.M. Feist, Palsson BØ, S.Y. Lee, Genome-scale reconstruction and in silico analysis of the *Clostridium acetobutylicum* ATCC 824 metabolic network, Appl. Microbiol. Biotechnol. 80 (2008) 849–862.
[21] J. Nolling, G. Breton, M.V. Omelchenko, K.S. Makarova, Q. Zeng, R. Gibson, et al., Genome sequence and comparative analysis of the solvent-producing bacterium *Clostridium acetobutylicum*, J. Bacteriol. 183 (2001) 4823–4838.
[22] R.A. Azevedo, P.J. Lea, Lysine metabolism in higher plants, Amino Acids 20 (2001) 261–279.
[23] A. Kaplun, M. Vyazmensky, Y. Zherdev, I. Belenky, A. Slutzker, S. Mendel, et al., Structure of the regulatory subunit of acetohydroxyacid synthase isozyme III from *Escherichia coli*, J. Mol. Biol. (2006).
[24] D.M. Chipman, B.A.C.T. Shaanan The, Domain family, Curr. Opin. Struct. Biol. 11 (2001) 694–700.
[25] R. Dumas, D. Cobessi, A.Y. Robin, J.-L. Ferrer, G. Curien, The many faces of aspartate kinases, Arch. Biochem. Biophys. 519 (2012) 186–193.
[26] M. Kotaka, J. Ren, M. Lockyer, A.R. Hawkins, D.K. Stammers, Structures of R- and T-state *Escherichia coli* aspartokinase III. Mechanisms of the allosteric transition and inhibition by lysine, J. Biol. Chem. 281 (2006) 31544–31552.
[27] X. Liu, A.G. Pavlovsky, R.E. Viola, The structural basis for allosteric inhibition of a threonine-sensitive Aspartokinase, J. Biol. Chem. 283 (2008) 16216–16225.
[28] C. Mas-Droux, G. Curien, M. Robert-Genthon, M. Laurencin, J.L. Ferrer, R. Dumas, A novel organization of ACT domains in allosteric enzymes revealed by the crystal structure of Arabidopsis aspartate kinase, Plant Cell 18 (2006) 1681–1692.
[29] A. Yoshida, T. Tomita, T. Kuzuyama, M. Nishiyama, Mechanism of concerted inhibition of alpha2beta2-type hetero-oligomeric aspartate kinase from *Corynebacterium glutamicum*, J. Biol. Chem. 285 (2010) 27477–27486.
[30] C.M. Weeks, P.D. Adams, J. Berendzen, A.T. Brunger, E.J. Dodson, R.W. Grosse-Kunstleve, et al., Automatic solution of heavy-atom substructures, Meth. Enzymol. 374 (2003) 37–83.
[31] S. Ramon-Maiques, A. Marina, M. Uriarte, I. Fita, V. Rubio, The 1. 5 a resolution crystal structure of the carbamate kinase-like carbamoyl phosphate synthetase from the hyperthermophilic Archaeon pyrococcus furiosus, bound to ADP, confirms that this thermostable enzyme is a carbamate kinase, and provides insight into substrate binding and stability in carbamate kinases, J. Mol. Biol. 299 (2000) 463–476.
[32] L. Aravind, E.V. Koonin, Gleaning non-trivial structural, functional and evolutionary information about proteins by iterative database searches, J. Mol. Biol. 287 (1999) 1023–1040.
[33] J.S. Liberles, M. Thórólfsson, A. Martínez, Allosteric mechanisms in ACT domain containing enzymes involved in amino acid metabolism, Amino Acids 28 (2005) 1–12.
[34] Q. Yang, K. Yu, L. Yan, Y. Li, C. Chen, X. Li, Structural view of the regulatory subunit of aspartate kinase from *Mycobacterium tuberculosis*, Protein Cell 2 (2011) 745–754.
[35] D.J. Schuller, G.A. Grant, L.J. Banaszak, The allosteric ligand site in the Vmax-type cooperative enzyme phosphoglycerate dehydrogenase, Nat. Struct. Biol. 2 (1995) 69–76.
[36] P.J. Cross, T.M. Allison, R.C.J. Dobson, G.B. Jameson, E.J. Parker, Engineering allosteric control to an unregulated enzyme by transfer of a regulatory domain, Proc. Natl. Acad. Sci. U.S.A. 110 (2013) 2111–2116.
[37] C. Richaud, J.P. Mazat, C. Gros, J.C. Patte, Subunit structure of aspartokinase 3 of *Escherichia coli* K12, Eur. J. Biochem. 40 (1973) 619–629.
[38] C.R. Faehnle, X. Liu, A. Pavlovsky, R.E. Viola, The initial step in the archaeal aspartate biosynthetic pathway catalyzed by a monofunctional aspartokinase, Acta Crystallogr. Sect. F Struct. Biol. Cryst. Commun. 62 (2006) 962–966.
[39] Y. Ogawa-Miyata, H. Kojima, K. Sano, Mutation analysis of the feedback inhibition site of aspartokinase III of *Escherichia coli* K-12 and its use in L-threonine production, Biosci. Biotechnol. Biochem. 65 (2001) 1149–1154.
[40] Z. Chen, S. Rappert, J. Sun, A.P. Zeng, Integrating molecular dynamics and co-evolutionary analysis for reliable target prediction and deregulation of the allosteric inhibition of aspartokinase for amino acid production, J. Biotechnol. 154 (2011) 248–254.
[41] C. Marco-Marin, S. Ramon-Maiques, S. Tavarez, V. Rubio, Site-directed mutagenesis of *Escherichia coli* acetylglutamate kinase and aspartokinase III probes the catalytic and substrate-binding mechanisms of these amino acid kinase family enzymes and allows three-dimensional modelling of aspartokinase, J. Mol. Biol. 334 (2003) 459–476.
[42] Q. Qi, J. Huang, J. Crowley, L. Ruschke, B.S. Goldman, L. Wen, et al., Metabolically engineered soybean seed with enhanced threonine levels: biochemical characterization and seed-specific expression of lysine-insensitive variants of aspartate kinases from the enteric bacterium Xenorhabdus bovienii, Plant Biotechnol. J. 9 (2011) 193–204.
[43] S. Ufaz, G. Galili, Improving the content of essential amino acids in crop plants: goals and opportunities, Plant Physiol. 147 (2008) 954–961.
[44] M.R. Chance, A.R. Bresnick, S.K. Burley, J.S. Jiang, C.D. Lima, A. Sali, et al., Structural genomics: a pipeline for providing structures for the biologist, Protein Sci. 11 (2002) 723–738.

[45] B.A. Manjasetty, W. Shi, C. Zhan, A. Fiser, M.R. Chance, A high-throughput approach to protein structure analysis, Genet. Eng. (NY) 28 (2007) 105–128.
[46] M.J. Sauder, M.E. Rutter, K. Bain, I. Rooney, T. Gheyi, S. Atwell, et al., High throughput protein production and crystallization at NYSGXRC, Meth. Mol. Biol. 426 (2008) 561–575.
[47] Z. Otwinowski, W. Minor, Processing of X-ray diffraction data collected in oscillation mode, Meth. Enzymol. 276 (1997) 307–326.
[48] B.W. Matthews, Solvent content of protein crystals, J. Mol. Biol. 33 (1968) 491–497.
[49] T.R. Schneider, G.M. Sheldrick, Substructure solution with SHELXD, Acta Crystallogr. D Biol. Crystallogr. 58 (2002) 1772–1779.
[50] T.C. Terwilliger, J.M.A.D. Berendzen Automated, MIR structure solution, Acta Crystallogr. D-Biol. Cryst. 55 (1999) 849–861.
[51] T.C. Terwilliger, Maximum-likelihood density modification using pattern recognition of structural motifs, Acta Crystallogr. D Biol. Crystallogr. 57 (2001) 1755–1762.
[52] S. Panjikar, V. Parthasarathy, V.S. Lamzin, M.S. Weiss, P.A. Tucker, On the combination of molecular replacement and single-wavelength anomalous diffraction phasing for automated structure determination, Acta Crystallogr. D Biol. Crystallogr. 65 (2009) 1089–1097.
[53] P. Emsley, K. Cowtan Coot:, Model-building tools for molecular graphics, Acta Crystallogr. D Biol. Crystallogr. 60 (2004) 2126–2132.
[54] Collaborative Computational Project Number 4CCPN. The CCP4 suite: programs for protein crystallography. Acta Crystallogr. Sect. D, Biol. Crystallogr. 1994;50:760–3.
[55] G.N. Murshudov, A.A. Vagin, E.J. Dodson, Refinement of macromolecular structures by the maximum-likelihood method, Acta Crystallogr. Sect. D Biol. Crystallogr. 53 (1997) 240–255.
[56] R.A. Laskowski, M.W. MacArthur, D.S. Moss, J.M. Thornton PROCHECK:, A program to check the stereochemical quality of protein structures, J. Appl. Crystallogr. 26 (1993) 283–291.
[57] E. Krissinel, K. Henrick, Inference of macromolecular assemblies from crystalline state, J. Mol. Biol. 372 (2007) 774–797.
[58] R.A. Lee, M. Razaz, S. Hayward, The DynDom database of protein domain motions, Bioinformatics 19 (2003) 1290–1291.
[59] Z. Li, H. Wan, Y. Shi, P. Ouyang, Personal experience with four kinds of chemical structure drawing software: review on ChemDraw, ChemWindow, ISIS/Draw, and ChemSketch, J. Chem. Inf. Comput. Sci. 44 (2004) 1886–1890.
[60] R. Chenna, H. Sugawara, T. Koike, R. Lopez, T.J. Gibson, D.G. Higgins, et al., Multiple sequence alignment with the Clustal series of programs, Nucleic Acids Res. 31 (2003) 3497–3500.